Insights into Gas Hydrate Dynamics from 3D Seismic Data, Offshore Mauritania

27

Christian Berndt, Richard Davies, Ang Li, and Jinxiu Yang

Abstract

The gas hydrate system off Mauritania is characterized by the undulating landward termination of a gas hydrate-related bottom simulating reflector (BSR). Some of the most landward sections of this BSR reach up to within 6 m of the seafloor. This suggests a shallow sulphate-methane-interface over an unusually large area. We attribute this to the presence of large amounts of methane due to the efficient burial of organic matter in a high-productivity oceanographic region, and the efficient channelling of methane along permeable turbidite beds towards the feather edge of the gas hydrate stability zone. This is consistent with the observation of steps in the BSR, where it cross-cuts other inferred permeable horizons. The high thermal conductivity of a salt dome in the southern part of the study area distorts the subsurface temperature field, giving the base of the hydrate stability zone a concave-down shape. Within this anticline of the BSR, high amplitudes and a horizontal reflection that crosses the sedimentary strata indicate the entrapment of free gas. We interpret this as a direct indication of a reduced hydraulic permeability of the hydrate-bearing sediment.

C. Berndt (✉)
GEOMAR Helmholtz Centre for Ocean Research, Kiel, Germany
e-mail: cberndt@geomar.de

R. Davies
Newcastle University, Newcastle upon Tyne, UK

A. Li
Qingdao Institute of Marine Geology, Qingdao, China

J. Yang
School of Geosciences, China University of Petroleum, Qingdao, China

27.1 Introduction

The gas hydrate province off Mauritania (Fig. 27.1) has attracted little scientific attention, despite the presence of a well-developed bottom simulating reflector (BSR) in the area. No marine geological expeditions dedicated to hydrate research have been conducted on the Mauritanian Margin until now; all of the information available on this hydrate system stems from the seismic data collected by the hydrocarbon industry.

Former PhD candidates Jinxiu Yang (2013) and Ang Li (2017) carried out their PhD projects at Durham University in the early 2010s. Both projects involved the analysis of two large 3D seismic cubes, collected off Mauritania from blocks C-19 and C-6 (Fig. 27.1). These studies focused on the role of gas hydrates on slope stability (Li et al. 2016; Yang et al. 2013), the role of the hydrate system in buffering methane flux in times of climate change, the role of hydrates for gas migration at the intersection of the gas hydrate stability zone (GHSZ) and the seabed (Davies et al. 2015), and the role of hydrate formation at the base of the hydrate stability zone for fluid migration pathways (Davies et al. 2014).

This article summarizes the results of these studies with an emphasis on the geological conditions that provide for a BSR located unusually close to the seafloor, the role of salt diapirs for the thermal state of the basin and the effects of gas hydrates on the hydraulic permeability of sediment.

27.2 Geological Setting

The Northwest African Continental Margin is the result of a Late Jurassic rifting between Africa and North America and the subsequent continental breakup around 155 Ma (Rad et al. 1982; Seton et al. 2012). During early post-rift history, evaporites were deposited along the Mauritanian Margin

J. Mienert et al. (eds.), *World Atlas of Submarine Gas Hydrates in Continental Margins*,
https://doi.org/10.1007/978-3-030-81186-0_27

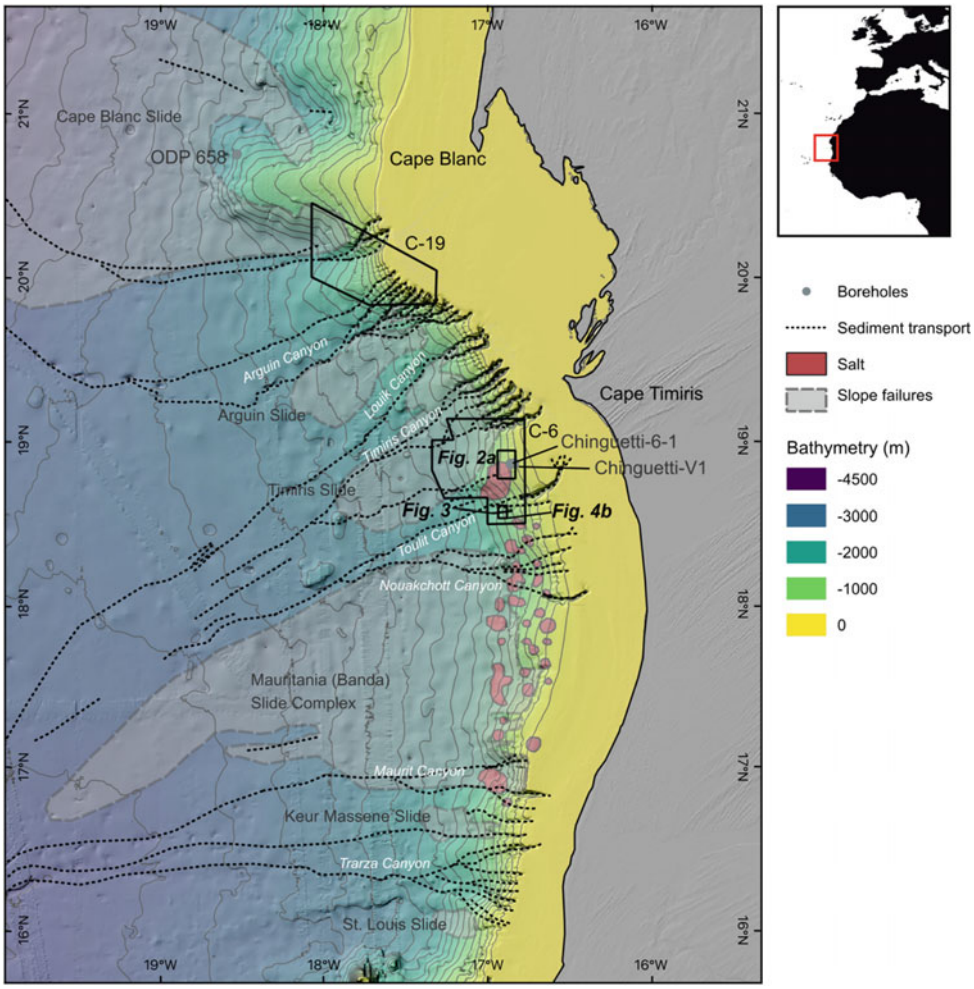

Fig. 27.1 Geological setting of the gas hydrate province off Mauritania. Sediment transport pathways and submarine slope failures were adapted from (Krastel et al. 2006) and (Wienberg et al. 2018) and updated with the GEBCO-2019 bathymetry (background). Black polygons show the extent of exploration 3D seismic data and location of Figs. 27.2a, 27.3 and 27.4b. Outline of salt diapirs after Soto et al. 2017

within the Senegal Basin (Weigel et al. 1982). While the rift basins were initially filled by fluvial input from the Senegal River in the south and another drainage system north of Cape Timiris (Vörösmarty et al. 2000), Holocene sedimentation is predominantly aeolian as trade winds transport dust from the Sahara Desert westward and offshore (Koopmann 1981). Together with the upwelling of cold water, this leads to particularly high biological productivity and a significant burial of organic matter (Müller and Suess 1979). Today, the continental margin is shaped by down-slope sediment transport through canyons (Krastel et al. 2019; Weaver 2003; Wynn et al. 2000) and by large open-slope landslides (Antobreh and Krastel 2006; Henrich et al. 2008) (Fig. 27.1). Cold water coral reefs have additionally been discovered at the shelf break, attracting recent academic attention (Wienberg et al. 2018). Hydrocarbon exploration wells (Chinguetti-6–1 and Chinguetti-V1; Fig. 27.1) show that the uppermost sediment hosting the gas hydrate system has been deposited over the past 5 myrs, consisting of fine-grained turbidites and nannofossil-rich muds (Davies et al. 2015).

27.3 Data

The aforementioned PhD theses were based on two high-quality exploration 3D seismic cubes, acquired from block C-6 in March 2000 and from block C-19 in December 2012 (Fig. 27.1). They were provided to Durham University by Petronas, Tullow Oil and their partners. The data from block C-19 were acquired by Fugro Geoteam using 12 streamers with 564 channels and a group interval of 12.5 m. The streamers were towed at a nominal distance of 100 m apart at 8 m depth. Two airgun sources were towed 50 m apart at 6 m depth, with a shot point interval of 25 m. Processing of the data involved multiple suppression, FX-deconvolution and Kirchhoff pre-stack depth migration with 12.5 m × 25 m bin size, using a velocity field derived by a three-pass tomographic velocity inversion. The data were then stretched back to two-way travel time and displayed with an AGC after a wavelet domain denoise filter. The data from block C-6 (Figs. 27.2, 27.3, 27.4) were processed using a post-stack time migration on a 25 × 25 m grid.

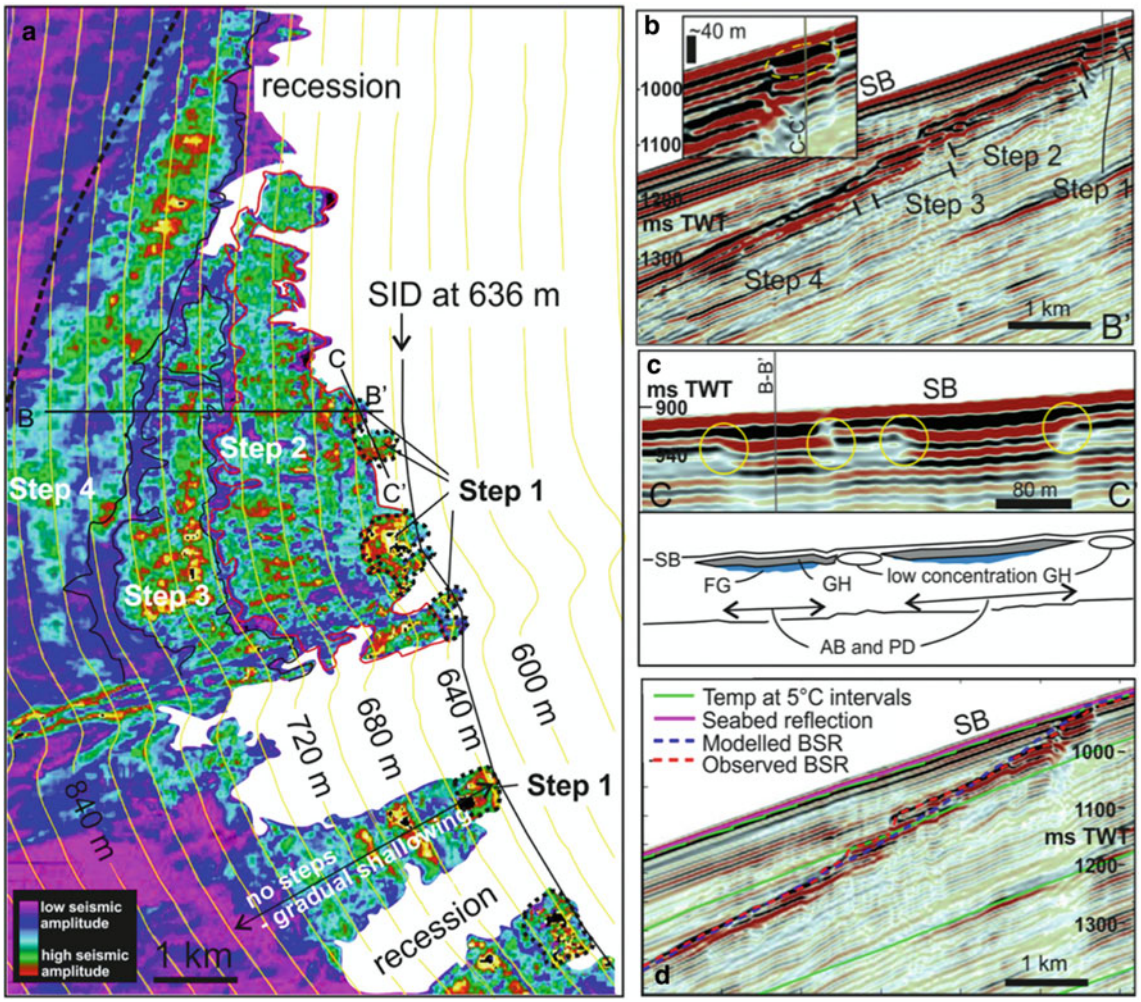

Fig. 27.2 **a** RMS seismic amplitudes for the BSR in the feather edge region (i.e., the eastern termination) marks the intersection of the BSR and the seafloor. Yellow contour lines indicate water depth. Note the bands of low RMS amplitude that are related to the steps in the BSR (also seen in (**b**) and (**d**)). **b** and **d** seismic line B-B' in (**a**), showing the BSR very close to the seafloor. Note the tuning effect in inset in (b) caused by interference of the BSR reflection and the seafloor reflection, indicating that the BSR is reaching up to the seafloor to within the range of seismic resolution (i.e., approximately 6 m). The green lines in (**d**) are isotherms of the thermal model that was used to calculate the theoretical BSR depth (dashed blue line) for pure methane gas composition at a geothermal gradient of 32ºC km^{-1} and 35 PSU pore water salinity. **c** seismic line across the feather edge C–C' in (**a**). From Davies et al. 2015, for location see Fig. 27.1

To estimate the temperature perturbation caused by the high thermal conductivity of the salt, a 2D steady state heat-flow model was used to calculate subsurface temperatures in the same way as Hornbach et al.'s model for the Blake Ridge Diapir (Hornbach et al. 2005). We used 6 Wm^{-1} K^{-1} thermal conductivity of salt and 1 Wm^{-1} K^{-1} for the background sediments, with a hydrostatic pressure gradient of 10.09 MPa km^{-1} and isotropic and homogenous heat conductivities. The bottom water temperature was taken from Davies et al. (2014), and a geothermal gradient of 32ºC km^{-1} was used for the background away from the salt diapir. The specific heat capacity was taken at 220 JK^{-1} kg^{-1}. We used a pure methane gas composition and pore water salinity at 35 PSU. Further details on the thermal modelling are found in Li et al. (2017).

27.4 Observations

The 3D seismic data show a BSR that is approaching the seafloor at several parts of the feather edge region (Fig. 27.2). The BSR is characterized by a band of high-amplitude reflections that are between 10 and 40 ms TWT long and laterally variable. The seafloor reflection consists of a weak negative, a strong positive (red) and a medium negative phase, indicating that it is a minimum or

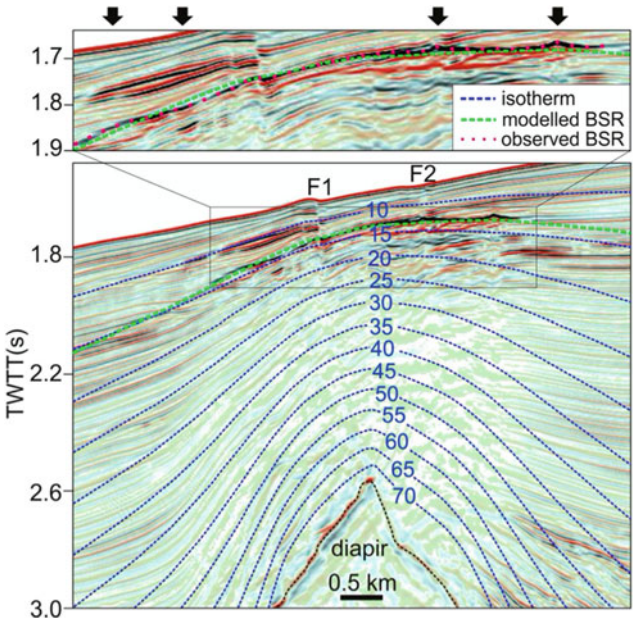

Fig. 27.3 Distortion of subsurface temperatures due to a salt diapir. Note the upwarped BSR about 100 ms TWT below the seafloor and two faults (F1, F2) forming and graben structure above the crest of the diapir. The observed BSR and the calculated base of the gas hydrate stability zone match very well. From Li 2017, for location see Fig. 27.1

mixed phase. The strongest phase of the BSR is negative (black), indicating that it is the result of a decrease in acoustic impedance. Together with its high amplitude, this suggests that it is underlain by free gas. The greater number of phases of the BSR reflection compared to the seafloor implies that the seismic resolution is sufficient to resolve several gas-bearing horizons. At a lower resolution. the BSR would consist of a single reverse polarity event. Apart from the very shallow depth of the BSR at its landward termination, there are two more interesting observations. First, there is a tuning effect at the intersection of the BSR and the seafloor (Fig. 27.2b–d), which implies that the free gas is less than a quarter of the wavelength (in this case about 6 m) below the seafloor (Taner and Sheriff 1977). Second, the BSR is characterized by steps that can be seen in both the seismic lines (Fig. 27.2b, d) and in the root mean square (RMS) amplitude map (Fig. 27.2a).

In the southern part of the study area, a strong positive polarity seismic reflection is visible at 2.6–3.0 s TWT (Fig. 27.3). It forms a ridge structure that dips downwards in both directions. The overlying sedimentary strata are bent upwards above this ridge, and two faults form a graben structure above the tip of the strong reflection. The western fault clearly offsets the seafloor, while the eastern fault affects the seafloor only gently. The BSR is visible as a cross-cutting reverse polarity event approximately 100 ms TWT below the seafloor (dashed red line in Fig. 27.3). The lower panel of Fig. 27.3 shows the steady-state isotherms (blue dashed lines), which are calculated based on the assumption that the strong amplitude event at 2.6 s TWT is the top of a salt diapir, including the parameterization already described. The isotherms are deflected upward due to the high thermal conductivity of the interpreted salt diapir. The calculated depth of the base of the hydrate stability zone (green dashed line) coincides very well with the observed BSR and has an up-warped shape.

The outline of the up-warped area is visible on an RMS amplitude map of the BSR (Fig. 27.4b). The anomaly extends for about 12 km in a N-S direction, and between 8 km in the north and 5 km in the south in an E-W direction. The highest amplitudes coincide with the crest of the up-warped area that strikes in a N/NW-S/SE direction. The upwarped BSR is underlain by a normal polarity event (red phase in Figs. 27.3 and 27.4) in its southernmost section, showing the typical characteristics of a flat spot (i.e., it is cross-cutting the sedimentary reflections and it is horizontal apart from a slight delay where the overlying high amplitudes are thickest). The arrival is bound by the BSR in the west and terminates against a sedimentary reflection in the east, precisely where the overlying high amplitude reflections stop.

27.5 Discussion

27.5.1 Reasons for Very Shallow BSRs

BSRs are generally caused by the drop in acoustic impedance due to the presence of free gas below the base of the gas hydrate stability zone (Pecher et al. 1996). Except for some particularly highly-saturated hydrate accumulations (e.g., Fujii et al. 2016), the hydrates themselves are not easily detectable in the seismic data. A common observation is that the BSR does not reach all the way to the seafloor, where the base of the hydrate stability zone and the seafloor intersect (e.g., Mienert et al. 2005; Phrampus and Hornbach 2012; Sarkar et al. 2012). While this may be coincidental (e.g., due to lateral lithological changes or changes in gas supply), the omnipresence of this observation suggests that the lack of a BSR at a very shallow depth is caused by the biological consumption of methane.

Microbial communities are able to oxidize methane under anaerobic conditions (Boetius et al. 2000) using sulphate that is diffusively migrating downward from the water column. This biological process reduces the sulphate concentration downward and the methane concentration upward. The depth at which the sulphate and methane concentrations approach their minimum is called the methane sulphate transition zone (Hensen et al. 2003). While the downward flux of sulphate is largely controlled by diffusion and is fairly constant, the upward advection of methane can vary

significantly, controlling the depth of the sulphate methane transition at active gas vent sites. This depth variation can range from a few centimetres (Treude et al. 2020) to 10–20 m below the seafloor for areas without methane advection (Coffin et al. 2007). In rare cases of downward sulphate transport by fluid migration, the sulphate methane transition can be as deep as several hundred meters (Gay et al. 2010). Unfortunately, no sediment cores exist to our knowledge from the landward termination of the hydrate stability zone offshore Mauritania that would allow for a direct observation of the sulphate methane transition zone depth.

The high productivity at the Mauritanian Margin, caused by the aeolian transport of Sahara sand and the upwelling of oxygen-rich deep water masses, leads to the efficient burial of organic matter (Müller and Suess 1979), which is likely the dominant source of biogenic methane production in this area. Therefore, the occurrence of the particularly shallow BSR off Mauritania is likely due to high background methane production and advection. Furthermore, the steps in BSR depth (Fig. 27.2b, d) suggest that the methane flux is focused along particularly permeable sedimentary units (e.g., turbidite layers) that are sandier than the surrounding sediments, showing a higher hydraulic permeability. The presence or absence of such beds would control the fluid pathways and explain both the steps in the BSR and recessions of the BSR where the permeable beds are absent (Davies et al. 2015) (Fig. 27.2a).

27.5.2 Thermal Effects of Salt Diapirs on Hydrate Stability

The presence of evaporite deposits on the Mauritanian Margin has been known since the early days of seismic exploration (Weigel et al. 1982). Although recent maps do not indicate salt in the southern part of the study area (Fig. 27.1), the seismic characteristics of the strong positive polarity reflector and the seismic reflector configuration on both sides of its crest (typical for sag basins) suggest that there is a salt diapir in the southern part of the study area. The observation of typical crest faults (Fig. 27.3) and its location between two mapped salt diapirs (Fig. 27.1) supports this interpretation.

Calculating the effects of a salt diapir on the thermal state of the basin, assuming a steady state and using the parameterization previously described, allows for the calculation of the depth of the base of the hydrate stability zone (Fig. 27.3 top panel). The striking match between this calculated base and the observed BSR above the salt diapir supports the interpretation of a salt diapir and the significant match away from the crest of the diapir. This is despite the fact that we do not take the three-dimensional geometry variations of the salt diapir into consideration, suggesting that the parameterization is good. The high thermal conductivity of salt leads to increased subsurface temperatures in its overburden. The temperatures are about 30ºC higher directly above the diapir than at similar sub-bottom depths away from the diapir (Fig. 27.3). A similar effect was observed for the Blake Ridge Diapir (Hornbach et al. 2005). The strongest perturbation of the sub-bottom temperatures occurs directly above the diapir, and the effect is superposed onto the regional geothermal gradient.

27.5.3 Effects of Gas Hydrates on the Effective Permeability of Gas

As the seabed in the study area slopes only gently towards the west, the salt diapir-induced elevated subsurface temperatures cause the base of the gas hydrate stability zone to assume a concave-down shape. Within the southern part of the study area above the salt diapir (Fig. 27.1), the thermal disturbance thus creates a four-way closure by hydrate formation. The outline of this four-way closure can be seen by map view in Fig. 27.4b Seismic line X-X' (Fig. 27.4a) shows that gas, as represented by the high amplitude reflections between the BSR and the flat spot, has accumulated below the BSR. The BSR (top of gas) has a reverse polarity, whereas the flat spot has a normal polarity with respect to the seafloor. The flat spot terminates onto sedimentary reflectors in the east, probably representing less porous strata that do not host gas in sufficient quantities to be visible in the seismic data.

The fact that gas accumulates below the BSR and forms a gas reservoir is direct evidence that the presence of gas hydrates in the pore space sufficiently reduce the hydraulic permeability required to capture gas. The height of the gas column is a direct measure for the minimum overpressure that this pressure seal can withstand (Hornbach et al. 2004). As overpressure reduces the effective stress, the slopes will destabilize.

27.6 Conclusions

The gas hydrate province off Mauritania is characterized by a BSR that reaches unusually high towards the seafloor at the landward termination of the gas hydrate stability zone. We attribute this to large amounts of methane within northwest Africa's high productivity zone, which is augmented by sediment properties that funnel methane towards the feather edge. This indicates that the Mauritanian Margin hosts significant amounts of gas hydrates in the shallowest parts of the gas hydrate stability zone, which is most sensitive to climate change (Berndt et al. 2014; Phrampus and Hornbach 2012).

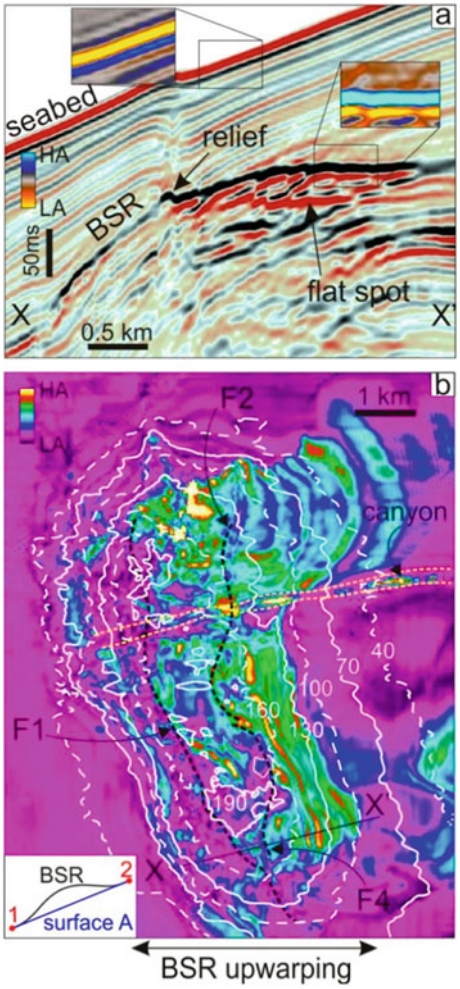

Fig. 27.4 Gas entrapment underneath an up-warped BSR. The horizontal red phase marked flat spot is interpreted as a gas–water contact due to charging of the trap formed by the concave down shape of the gas hydrate stability zone. Insets show the phase reversal of the BSR consistent with a hydrate-gas contact. From Li 2017, for location see Fig. 27.1

Salt diapir-related subsurface temperature perturbations have caused a trap for gas below a concave-down BSR. The ability of gas hydrates to trap free gas in this region means that they must have a strong effect on sediment permeability, most likely because they cement the sediment grains. This causes an increase in overpressure at shallow depths, potentially posing a drilling hazard and weakening the stability of the slope.

Acknowledgements We thank Elsevier for permission to reproduce Fig. 27.2 from Davies et al. (2015). 3D seismic data were made available by Petronas and Tullow Oil.

References

Antobreh AA, Krastel S (2006) Mauritania slide complex: morphology, seismic characterisation and processes of formation. Int J Earth Sci (geol Rundsch) 96:451–472. https://doi.org/10.1007/s00531-006-0112-8

Berndt C, Feseker T, Treude T et al (2014) Temporal constraints on hydrate-controlled methane seepage off Svalbard. Science 343:284–287. https://doi.org/10.1126/science.1246298

Boetius A, Ravenschlag K, Schubert CJ et al (2000) A marine microbial consortium apparently mediating anaerobic oxidation of methane. Nature 407:623–626. https://doi.org/10.1038/35036572

Coffin R, Pohlman J, Gardner J et al (2007) Methane hydrate exploration on the mid Chilean coast: a geochemical and geophysical survey. J Pet Sci Eng 56:32–41. https://doi.org/10.1016/j.petrol.2006.01.013

Davies RJ, Yang J, Hobbs R et al (2014) Probable patterns of gas flow and hydrate accretion at the base of the hydrate stability zone. Geology 42:1055–1058. https://doi.org/10.1130/G36047.1

Davies RJ, Yang J, Li A et al (2015) An irregular feather-edge and potential outcrop of marine gas hydrate along the Mauritanian margin. Earth Planet Sci Lett 423:202–209. https://doi.org/10.1016/j.epsl.2015.04.013

Fujii T, Tin Aung T, Wada N et al (2016) Modeling gas hydrate petroleum systems of the Pleistocene turbiditic sedimentary sequences of the Daini-Atsumi area, eastern Nankai Trough, Japan. Interpretation 4:SA95–SA111. http://doi.org/https://doi.org/10.1190/INT-2015-0022.1

Gay A, Takano Y, Gilhooly Iii WP et al (2010) Geophysical and geochemical evidence of large scale fluid flow within shallow sediments in the eastern Gulf of Mexico, offshore Louisiana. Geofluids 11:34–47. https://doi.org/10.1111/j.1468-8123.2010.00304.x

Henrich R, Hanebuth TJJ, Krastel S et al (2008) Architecture and sediment dynamics of the Mauritania Slide Complex. Mar Pet Geol 25:17–33. https://doi.org/10.1016/j.marpetgeo.2007.05.008

Hensen C, Zabel M, Pfeifer K et al (2003) Control of sulfate pore-water profiles by sedimentary events and the significance of anaerobic oxidation of methane for the burial of sulfur in marine sediments. Geochim Cosmochim Acta 67:2631–2647. https://doi.org/10.1016/S0016-7037(03)00199-6

Hornbach MJ, Saffer DM, Steven Holbrook W (2004) Critically pressured free-gas reservoirs below gas-hydrate provinces. Nature 427:142–144. https://doi.org/10.1038/nature02172

Hornbach MJ, Ruppel C, Saffer DM et al (2005) Coupled geophysical constraints on heat flow and fluid flux at a salt diapir. Geophys Res Lett 32:325–334. https://doi.org/10.1029/2005GL024862

Koopmann B (1981) Sedimentation von Saharastaub im subtropischen Nordatlantik während der letzten 25.000 Jahre. Meteor Forschungs-Ergebnisse 23–59

Krastel S, Wynn RB, Hanebuth TJJ et al (2006) Mapping of seabed morphology and shallow sediment structure of the Mauritania continental margin, Northwest Africa: some implications for geohazard. Nor J Geol 86:163–176

Krastel S, Li W, Urlaub M et al (2019) Mass wasting along the NW African continental margin. Geol Soc, London, Spec Pub 477:151–167. https://doi.org/10.1144/SP477.36

Li A (2017) Three-dimensional seismic analysis and modelling of marine hydrate systems offshore of Mauritania. PhD Thesis, Durham University

Li A, Davies RJ, Yang J (2016) Gas trapped below hydrate as a primer for submarine slope failures. Mar Geol 380:264–271. https://doi.org/10.1016/j.margeo.2016.04.010

Li A, Davies RJ, Mathias SA et al (2017) Gas venting that bypasses the feather edge of marine hydrate, offshore Mauritania. Mar Pet Geolg 88:402–409. https://doi.org/10.1016/j.marpetgeo.2017.08.026

Mienert J, Vanneste M, Bünz S et al (2005) Ocean warming and gas hydrate stability on the mid-Norwegian margin at the Storegga Slide. Mar Pet Geol 22:233–244

Müller PJ, Suess E (1979) Productivity, sedimentation rate, and sedimentary organic matter in the oceans—I. Organic carbon preservation. Deep Sea Res Part i: Oceanogr Res Pap 26:1347–1362. https://doi.org/10.1016/0198-0149(79)90003-7

Pecher IA, Minshull TA, Singh SC et al (1996) Velocity structure of a bottom simulating reflector offshore Peru: results from full waveform inversion. Earth Planet Sci Lett 139:459–469. https://doi.org/10.1016/0012-821X(95)00242-5

Phrampus BJ, Hornbach MJ (2012) Recent changes to the Gulf Stream causing widespread gas hydrate destabilization. Nature 490:527–530. https://doi.org/10.1038/nature11528

Sarkar S, Berndt C, Minshull TA, et al (2012) Seismic evidence for shallow gas-escape features associated with a retreating gas hydrate zone offshore west Svalbard. J Geophys Res 117. https://doi.org/10.1029/2011JB009126

Seton M, Müller RD, Zahirovic S et al (2012) Global continental and ocean basin reconstructions since 200Ma. Earth-Sci Rev 113:212–270. https://doi.org/10.1016/j.earscirev.2012.03.002

Soto JI, Flinch JF, Tari G (2017) Permo-Triassic salt provinces of Europe, North Africa and the Atlantic Margins. In: Soto JI, Flinch JF (eds). Elsevier, Amsterdam

Taner MT, Sheriff RE (1977) Application of amplitude, frequency, and other attributes to stratigraphic and hydrocarbon determination. In: Seismic stratigraphy—applications to hydrocarbon exploration. Ame Assoc Pet Geol 301–327

Treude T, Krause S, Steinle L et al (2020) Biogeochemical consequences of nonvertical methane transport in sediment offshore Northwestern Svalbard. J Geophys Res Biogeosci 125:63. https://doi.org/10.1029/2019JG005371

von Rad U, Hinz K, Sarnthein M et al (1982) Geology of the Northwest African Continental Margin. Springer, Heidelberg

Vörösmarty CJ, Fekete BM, Global MM et al (2000) Global system of rivers: Its role in organizing continental land mass and defining land-to-ocean linkages. Global Biogeochem Cycles 14:599–621

Weaver PPE (2003) Northwest African continental margin: history of sediment accumulation, landslide deposits, and hiatuses as revealed by drilling the Madeira Abyssal Plain Paleoceanography 18.https://doi.org/10.1029/2002PA000758

Weigel W, Wissmann G, Goldflam P (1982) Deep seismic structure (Mauritania and Central Morocco). Geology of the Northwest African Margin. Springer, Berlin, pp 132–159

Wienberg C, Titschack J, Freiwald A et al (2018) The giant Mauritanian cold-water coral mound province: oxygen control on coral mound formation. Quat Sci Rev 185:135–152. https://doi.org/10.1016/j.quascirev.2018.02.012

Wynn RB, Masson DG, Stow DAV et al (2000) The Northwest African slope apron: a modern analogue for deep-water systems with complex seafloor topography. Mar Pet Geol 17:253–265. https://doi.org/10.1016/S0264-8172(99)00014-8

Yang JX (2013) 3D seismic analysis of subsurface gas migration and the gas hydrate system offshore Mauritania. PhD Thesis, Durham University

Yang J, Davies RJ, Huuse M (2013) Gas migration below gas hydrates controlled by mass transport complexes, offshore Mauritania. Mar Pet Geol 48:366–378. https://doi.org/10.1016/j.marpetgeo.2013.09.003